

UNCLE-Grasp: Uncertainty-Aware Grasping of Leaf-Occluded Strawberries

Malak Mansour, Ali Abouzeid, Zezhou Sun, Qinbo Sun, Dezhen Song, Abdalla Swikir

Department of Robotics, Mohamed bin Zayed University of Artificial Intelligence

Emails:{malak.mansour, ali.abouzeid, zezhou.sun, qinbo.sun, dezhen.song, abdalla.swikir}@mbzui.ac.ae

Abstract—Robotic strawberry harvesting is challenging under partial occlusion, where leaves induce significant geometric uncertainty and make grasp decisions based on a single deterministic shape estimate unreliable. From a single partial observation, multiple incompatible 3D completions may be plausible, causing grasps that appear feasible on one completion to fail on another. We propose an uncertainty-aware grasping pipeline for partially occluded strawberries that explicitly models completion uncertainty arising from both occlusion and learned shape reconstruction. Our approach uses point cloud completion with Monte Carlo dropout to sample multiple shape hypotheses, generates candidate grasps for each completion, and evaluates grasp feasibility using physically grounded force-closure-based metrics. Rather than selecting a grasp based on a single estimate, we aggregate feasibility across completions and apply a conservative lower confidence bound (LCB) criterion to decide whether a grasp should be attempted or safely abstained. We evaluate the proposed method in simulation and on a physical robot across increasing levels of synthetic and real leaf occlusion. Results show that uncertainty-aware decision making enables reliable abstention from high-risk grasp attempts under severe occlusion while maintaining robust grasp execution when geometric confidence is sufficient, outperforming deterministic baselines in both simulated and physical robot experiments.

I. INTRODUCTION

Robotic grasping in unstructured agricultural environments remains a challenging problem due to frequent occlusions, visual ambiguity, and partial observability of target objects. In fruit harvesting scenarios, strawberries are often partially covered by leaves, stems, or adjacent fruit, resulting in incomplete point cloud observations that can significantly distort geometric estimates. These errors propagate downstream to unstable or unreachable grasps, potentially resulting in fruit damage due to the robot's poor perception and unawareness of its own uncertainty. Harvesting is a sequential process: grasping surrounding fruit can reduce occlusion for subsequent targets, making uncertainty-aware decision making on heavily occluded strawberries preferable to premature grasp attempts.

Recent advances in learning-based grasp synthesis have demonstrated strong performance when accurate object geometry is available. Grasp prediction methods generate high-quality 6DoF grasps directly from point clouds; however, they implicitly assume that the observed geometry faithfully represents the underlying object. Under partial occlusion, this assumption no longer holds: grasp predictions become biased toward visible surfaces, leading to significant centroid shifts as occlusion increases (Fig. 1a). Furthermore, confidence scores

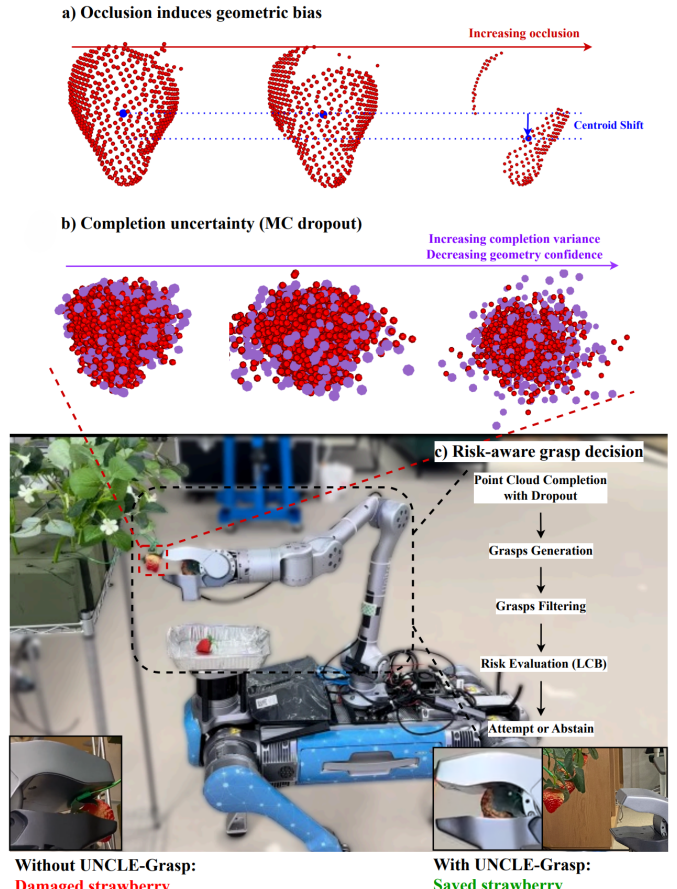


Fig. 1. Overview of UNCLE-Grasp: a) Increasing leaf occlusion induces centroid shift in the reconstructed point cloud. b) Completion uncertainty from MC shape completions increases with occlusion, reducing geometric confidence; purple regions indicate high uncertainty. c) Instead of selecting a single “best” grasp, UNCLE-Grasp evaluates object-level risk using LCB and either attempts to grasp the strawberry or abstains to avoid damaging it.

produced by deterministic grasp generating models fail to reflect the ambiguity introduced by missing geometry. As a result, grasp selection becomes brittle in heavily occluded scenes, motivating the need for explicit reasoning about uncertainty in downstream grasp decisions.

A common strategy to address partial observability and centroid shift is point cloud completion, where a model

TABLE I

COMPARISON WITH PRIOR WORK THAT ACCOUNTS FOR UNCERTAINTY IN GRASPING OR SHAPE COMPLETION. THE PROPOSED METHOD UNIQUELY PROPAGATES LEARNED SHAPE UNCERTAINTY INTO RISK-AWARE, OBJECT-LEVEL GRASP DECISIONS UNDER SEVERE OCCLUSION.

Capability	Pose Unc. [7]	Kehoe et al. [11]	Phys.-Based Unc. [13]	Ville et al. [5]	Diff. FC [4]	Humanoid Unc. [1]	Measuring Unc. [4]	PUGS [2]	UNCLE-Grasp
Learned Shape Completion	✗	✗	✗	✓	✗	✗	✓	✗	✓
Completion Uncertainty Modeling	✗	✗	✗	✓	✗	✗	✓	✗	✓
Uncertainty-Aware Grasp Evaluation	✓	✓	✓	✓	✗	✓	✗	✓	✓
Physically Grounded Grasp Feasibility	✓	✓	✓	✗	✓	✓	✗	✗	✓
Risk-Aware Bounds under Uncertainty	✗	✓	✓	✗	✗	✗	✗	✗	✓
Severe Occlusion Scenarios	✗	✗	✗	✓	✗	✗	✓	✓	✓
Object-Level Abstention	✗	✗	✗	✗	✗	✗	✗	✗	✓
Agricultural Harvesting	✗	✗	✗	✗	✗	✗	✗	✗	✓

reconstructs the full object shape from partial inputs. While completion can mitigate geometric bias, it introduces an additional source of uncertainty, as multiple possible completion models may result from the same partial observation. Most existing grasping pipelines treat the output of completion networks as deterministic, ignoring this inherent uncertainty and selecting grasps based on a single reconstructed shape. In safety-critical manipulation tasks such as harvesting delicate fruit, this overconfidence can lead to grasp failures, fruit damage, or unintended collisions with neighboring objects.

In this work, we propose an uncertainty-aware grasping pipeline for partially occluded strawberries that explicitly models uncertainty arising from both occlusion and learned shape completion. Our approach integrates transformer-based point cloud completion with Monte Carlo (MC) dropout to generate multiple plausible reconstructions of the occluded fruit. For each reconstructed shape, candidate grasps are generated and filtered using physically motivated geometric constraints, including collision-free jaw placement, stable grasp orientation, and front-facing, kinematically feasible approach directions. In addition to these deterministic checks, we apply uncertainty-aware filtering at two levels: highly uncertain grasps are removed based on local completion variance, and strawberries with consistently high uncertainty across completion samples are rejected at the object level. Rather than selecting a grasp based on mean confidence alone, we adopt a risk-aware Lower Confidence Bound (LCB) criterion to decide whether a strawberry should be grasped at all, jointly considering the expected grasp quality and its variance across shape completions.

In summary, this paper makes the following contributions:

- An uncertainty-aware grasping pipeline for partially occluded strawberries that combines learned point cloud completion with MC dropout to enable object-level abstention, avoiding grasp attempts on highly uncertain fruit.
- A physically grounded grasp filtering and evaluation framework that integrates geometric constraints with

uncertainty-aware grasp quality metrics to enable safe, risk-aware grasp selection under learned geometric uncertainty, and to systematically assess grasp reliability as occlusion severity of strawberries increases.

II. RELATED WORK

Our work spans robotic grasp synthesis in cluttered scenes, 3D shape completion from partial observations, and uncertainty-aware grasp planning. Table I summarizes key characteristics of representative prior approaches and highlights that our method uniquely integrates learned shape completion, explicit uncertainty modeling, and uncertainty-aware object-level grasp selection under severe occlusion.

A. Grasp Synthesis from Partial Observations

Early learning-based grasp synthesis methods such as GPD [22] and Dex-Net [17] generate robust grasps from point clouds or synthetic depth data, but typically assume access to reasonably complete object geometry. More recent approaches, including CGNet [21] and MVGrasp [10], operate directly on partial observations in clutter, with MVGrasp leveraging multi-view fusion to mitigate occlusions. While these methods reduce dependence on full geometry, they do not explicitly model geometric uncertainty induced by missing regions. In contrast, our approach uses shape completion and explicitly reasons about uncertainty in reconstructed geometry to enable risk-aware grasping under severe occlusion.

B. Shape Completion for Robotic Manipulation

To overcome the limitations of partial observations, shape completion has emerged as a key component for robotic manipulation. Early learning-based approaches reconstruct full object geometry from partial inputs using voxel-based representations [24, 3], but fixed-resolution grids limit scalability and the recovery of fine geometric detail.

More recent work explores expressive representations and uncertainty-aware completion. (author?) [20] proposes an implicit shape representation that provides confidence estimates

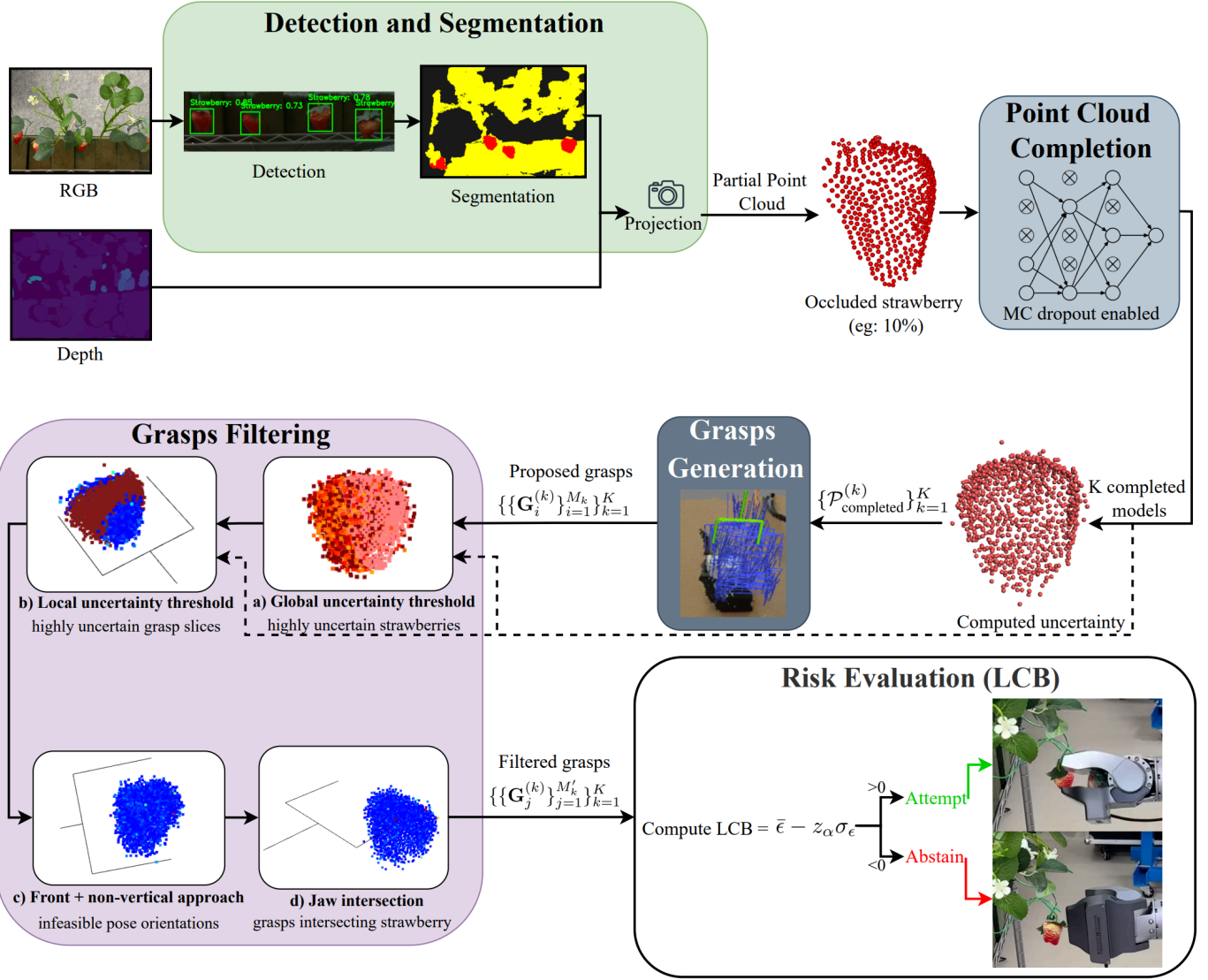


Fig. 2. Overview of the proposed uncertainty-aware strawberry grasping pipeline. Top: RGB input showing multiple strawberries partially occluded by leaves is detected and segmented, then 3D projected with the depth image to obtain a partial strawberry point cloud; A transformer-based point cloud completion network [23] reconstructs the missing geometry to produce the completed point cloud; MC dropout is enabled to generate K plausible completions $\{\mathcal{P}_{\text{completed}}^{(k)}\}_{k=1}^K$ and estimate geometric uncertainty. Middle: A grasps generation model [21] then takes each completed point cloud, $\mathcal{P}_{\text{completed}}^{(k)}$, and generates M grasps; The computed uncertainty from dropout is used to abstain from highly uncertain strawberries and filter through the grasp proposals using a) global and b) local uncertainty thresholds. Bottom: The remaining grasps are filtered using (c) orientation constraints (front-facing and non-vertical) and (d) jaw-object intersection checks. The filtered grasps from each completion sample k form the set M' , which are aggregated across all completion samples to compute an LCB-based feasibility score. A strawberry is attempted when $\text{LCB} > 0$; otherwise, the system abstains, enabling a higher grasp success rate.

for reconstructed points and allows resolution to be adjusted at inference time, while **(author?)** [8] explicitly predicts regions of high geometric uncertainty and demonstrates improved grasping by avoiding unreliable areas. Unlike these methods, which primarily use uncertainty at the local point or contact level, our approach integrates completion uncertainty into both local grasp filtering and object-level decision making by rejecting fruits with globally high uncertainty.

In the agricultural domain, **(author?)** [16] addresses fruit shape completion under heavy occlusion using a transformer-

based model that combines learned priors with deformable templates. While this work demonstrates the feasibility of shape completion under severe occlusion in realistic greenhouse environments, it does not propagate reconstruction uncertainty to risk-aware grasp filtering or object-level abstention based on geometric confidence.

C. Uncertainty-Aware Shape Completion and Grasp Planning

While shape completion enables reasoning beyond partial observations, uncertainty in the reconstructed geometry introduces additional challenges for downstream manipulation.

Early work on uncertainty-aware grasping builds on analytical grasp quality measures such as force closure, first formalized by (author?) [18], with (author?) [5] later introducing the widely used epsilon quality metric. Building on this foundation, (author?) [11] introduces one of the earliest formulations of grasp planning under shape uncertainty by estimating lower bounds on force-closure probability via MC sampling over parametric perturbations of a known object geometry. More recently, (author?) [14] introduces a differentiable force-closure estimator that enables efficient optimization of physically grounded grasp quality metrics under the assumption of known, deterministic object geometry. These formulations provide strong analytical guarantees, but either assume a fixed canonical object geometry or model uncertainty only through externally imposed parametric perturbations, and therefore do not address uncertainty arising from learned shape completion.

Subsequent work has explored physically grounded grasp evaluation under uncertainty assuming known or approximately known object geometry. Methods addressing pose uncertainty [7] and model perturbations [13] analyze the sensitivity of grasp stability to geometric variations, while more recent approaches incorporate uncertainty-aware grasp quality metrics to improve robustness [1]. While these methods provide principled uncertainty-aware grasp quality estimates, they assume access to a single underlying object geometry and do not address uncertainty arising from partial observability, which can lead to multiple incompatible completion hypotheses.

More closely related to our setting, learning-based approaches such as (author?) [15] use MC dropout at inference time to sample multiple plausible shape completions from partial observations, evaluating grasps across samples to improve robustness. Similarly, (author?) [4] shows that uncertainty-aware heuristics can improve grasp success rates by ranking grasps. In these works, uncertainty is treated as a perceptual signal or local heuristic, with dropout applied only at inference time and not to learn calibrated uncertainty during training, and is therefore not propagated into grasp feasibility bounds or object-level grasp decisions.

Uncertainty-aware grasp selection has also been explored in degraded sensing environments beyond terrestrial manipulation, such as underwater grasping [2]. While effective in their respective domains, these methods focus on uncertainty in perception or pose estimation rather than uncertainty arising from learned shape completion, where missing geometry can lead to multiple incompatible object hypotheses, and similarly do not consider object-level abstention.

Direct quantitative comparison with prior uncertainty-aware grasping methods is fundamentally invalid due to a mismatch in problem formulation and decision scope between them and UNCLE-Grasp (Table I). Existing approaches may estimate uncertainty from sensing noise or learned shape completion, but typically apply it at the grasp level, using local penalties or re-ranking strategies while still assuming that a grasp must be executed for every detected object. In contrast, our method operates under severe partial observability, where ge-

ometric uncertainty arises from learned shape completion and a single observation can admit multiple incompatible object hypotheses. This setting requires object-level decisions about whether a grasp should be attempted at all, which we address by aggregating feasibility across plausible completions and abstaining when geometric confidence is insufficient. Because prior benchmarks assume mandatory grasp execution and do not support object-level abstention under learned geometric ambiguity, they cannot meaningfully evaluate the risk-aware behavior that is central to our approach.

III. UNCERTAINTY-AWARE GRASPING PIPELINE

We propose an uncertainty-aware grasping framework designed to handle severe occlusion in agricultural environments. Rather than relying on a single deterministic estimate of object geometry, our pipeline propagates geometric uncertainty from stochastic shape completion through to a risk-aware, physically grounded grasp decision process based on LCB. While we demonstrate this approach using specific networks, the architecture is modular and compatible with any probabilistic completion or grasp synthesis model. The overall pipeline is illustrated in Fig. 2, and the algorithm is detailed in Appendix 1.

A. Point Cloud Completion with Dropout

Partial and occluded point clouds are completed using PointAttN [23], a transformer-based point cloud completion network that reconstructs missing geometry. Given a partial observation \mathcal{P} , the network produces a completed point cloud $\mathcal{P}_{\text{completed}}$.

To estimate geometric uncertainty under occlusion, we employ MC dropout in the completion network. Dropout is enabled during training, following the Bayesian interpretation of dropout as variational inference [6], to obtain well-calibrated uncertainty estimates. At inference time, enabling dropout yields K stochastic completions,

$$\{\mathcal{P}_{\text{completed}}^{(k)}\}_{k=1}^K, \quad (1)$$

from which we estimate per-point geometric uncertainty by computing the standard deviation of reconstructed point positions across samples.

This stochastic completion step directly supports our first contribution by explicitly modeling geometric uncertainty under occlusion and provides the basis for uncertainty-aware grasp generation and filtering, described next.

B. Grasp Generation and Filtering

1) *Grasp Generation*: For each completed point cloud $\mathcal{P}_{\text{completed}}^{(k)}$, we generate a set of candidate grasps using CGNet, which predicts 6-DoF grasp poses $\mathbf{G}_i^{(k)} \in \text{SE}(3)$ along with per-grasp confidence scores $s_i^{(k)}$.

Formally, grasp generation is given by

$$\{\mathbf{G}_i^{(k)}, s_i^{(k)}\}_{i=1}^{M_k} = \text{CGNet}(\mathcal{P}_{\text{completed}}^{(k)}), \quad (2)$$

where i indexes grasp candidates from 1 to M , number of grasps generated, for each completion sample k .

2) *Grasp Filtering Pipeline*: For each sample $k \in \{1, \dots, K\}$, we apply a multi-stage geometric and uncertainty-based filtering procedure:

a) *Global Uncertainty Filter*: To avoid grasp attempts on strawberries with highly ambiguous geometry, we apply a global uncertainty filter at the object level, as visualized in Grasp Filtering a) in Fig. 2. Using MC dropout, we generate K completed shapes per strawberry and compute a global geometric uncertainty measure that captures reconstruction consistency across samples. If the mean standard deviation of the points in the completion exceeds a threshold δ_{global} , the strawberry is rejected and no grasp is attempted, enabling safe abstention under high ambiguity.

b) *Local Uncertainty Filter*: For strawberries that pass the global uncertainty filter, we apply a local uncertainty filter at the grasp level. For each candidate grasp, we evaluate uncertainty in the contact regions by measuring the standard deviation of completed points within the corresponding grasp slice, as shown in Grasp Filtering b) in Fig. 2. Grasps whose local uncertainty exceeds a threshold δ_{local} are discarded, preventing reliance on unstable or inconsistent surface regions even when the overall object-level uncertainty is low.

c) *Approach Direction Filter*: A grasp is rejected if its approach vector (the negative z -axis of the grasp frame) does not approach the strawberry from its front, such as the sideways grasp in Grasp Filtering c) in Fig. 2, which could damage the fruit and the surrounding plant. The front approach filter can be formulated as

$$\text{grasp passes} \iff \mathbf{a}_i \cdot \mathbf{f} \geq \theta_{\text{dot}}, \quad (3)$$

where $\mathbf{a}_i = \mathbf{G}_i[0 : 3, 2]$ is the approach vector, \mathbf{f} is the front-facing direction, and θ_{dot} is the front-facing constraint's threshold.

d) *Vertical Grasp Filter*: Grasps with jaws aligned vertically (above each other), as shown in Grasp Filtering c) in Fig. 2, are rejected as unstable and formulated as

$$\text{grasp rejected} \iff |\mathbf{G}_i[0 : 3, 0] \cdot \mathbf{z}| > \theta_{\text{vert}}, \quad (4)$$

where \mathbf{z} is the world vertical axis and θ_{vert} is the vertically oriented grasp threshold. This vertical orientation constraint reflects the physical instability of vertically stacked finger configurations when grasping soft, approximately elliptical objects such as strawberries, which tend to slip in such orientations. The absolute value ensures that grasps are rejected whether the X-axis points up or down.

e) *Jaw-Object Intersection Test*: For each grasp, we verify that the gripper jaws do not intersect the object through a geometric clearance check to make sure the gripper jaws will not harm the strawberries as illustrated in Grasp Filtering d) in Fig. 2.

The jaw lines are

$$\mathbf{L}_{\text{left}} : \mathbf{c} - \frac{w}{2}\mathbf{x} + t\mathbf{a} \quad (5)$$

$$\mathbf{L}_{\text{right}} : \mathbf{c} + \frac{w}{2}\mathbf{x} + t\mathbf{a}, \quad (6)$$

where $\mathbf{c} = \mathbf{G}_i[0 : 3, 3]$ is the grasp center, $\mathbf{x} = \mathbf{G}_i[0 : 3, 0]$ is the jaw-opening direction, w is the gripper width, \mathbf{a} is the approach direction, and t is the jaw length.

A grasp is considered valid if no point in $\mathcal{P}_{\text{completed}}$ lies within a distance τ of either jaw line as formulated in

$$\text{grasp passes} \iff \forall \mathbf{p} \in \mathcal{P} : \min(d(\mathbf{p}, \mathbf{L}_{\text{left}}), d(\mathbf{p}, \mathbf{L}_{\text{right}})) > \tau. \quad (7)$$

This tolerance serves as a geometric clearance margin during collision checks against reconstructed point clouds, reflecting uncertainty in reconstruction accuracy and preventing gripper jaws from being placed too close to potentially inaccurate surface estimates.

Together, these filters realize the second contribution by eliminating unreliable grasps and enabling object-level abstention under high ambiguity. After filtering, only a subset M' of the original proposals M remains for each completion sample,

$$\{\mathbf{G}_j^{(k)}, s_j^{(k)}\}_{j=1}^{M'_k} \subseteq \{\mathbf{G}_i^{(k)}, s_i^{(k)}\}_{i=1}^{M_k}, \quad (8)$$

where $M' \leq M$. The remaining question is how to conservatively assess grasp feasibility across uncertain shape completions, which we address using physically grounded force-closure grasp quality metrics.

C. Grasp Quality Metrics

We evaluate grasp feasibility using the force-closure metric, which characterizes a grasp's ability to resist arbitrary external wrenches. Each contact contributes a friction cone parameterized by a friction coefficient μ , and the resulting contact wrenches form a convex set in wrench space. We use the ϵ metric, defined as the radius of the largest ball centered at the origin contained within this convex hull, with larger values indicating greater grasp robustness.

1) *Contact Estimation*: For each surviving grasp, we estimate the contact points by stepping along the approach direction until the jaw tips reach the point cloud surface. Given a grasp pose \mathbf{G} and jaw position trajectories, we compute contact points $\{\mathbf{c}_{\text{left}}, \mathbf{c}_{\text{right}}\}$ and their associated surface normals $\{\mathbf{n}_{\text{left}}, \mathbf{n}_{\text{right}}\}$ using nearest-neighbor queries.

2) *Grasp Epsilon Metric*: For each contact pair, we compute the grasp quality using the epsilon metric (force closure measure). The friction cone is discretized into N_{dir} directions, providing a conservative approximation that avoids overestimating grasp stability, particularly under uncertain contact conditions.

The grasp wrench matrix is constructed as

$$\mathbf{W} = \begin{bmatrix} \mathbf{F}_1 & \dots & \mathbf{F}_{2N_{\text{dir}}} \\ \tau_1 & \dots & \tau_{2N_{\text{dir}}} \end{bmatrix} \in \mathbb{R}^{6 \times 2N_{\text{dir}}}. \quad (9)$$

Each column of \mathbf{W} represents a 6D wrench. It consists of a contact force \mathbf{F}_j , corresponding to one discretized direction of the friction cone, applied at contact point \mathbf{c}_j . The resulting torque is given by $\tau_j = \mathbf{c}_j \times \mathbf{F}_j$.

The epsilon metric can be interpreted as the distance from the origin to the closest supporting hyperplane of the convex hull of feasible contact wrenches. Epsilon is represented as

$$\epsilon = \min_j \frac{|b_j|}{\|\mathbf{a}_j\|_2}, \quad (10)$$

where $\mathbf{a}_j^\top \mathbf{w} + b_j \leq 0$ denotes the j -th halfspace inequality describing the convex hull.

a) *Aggregation Across Uncertain Completions*: To use the ϵ metric as a feasibility signal under geometric uncertainty, we aggregate grasp quality estimates across MC-dropout completion samples. Letting $\{\mathbf{G}_j^{(k)}, s_j^{(k)}\}_{j=1}^{M'}$ denote the set of grasps that remain after filtering, we compute

$$\epsilon_k = \epsilon_{\text{metric}} \left(\bigcup_{i \in \{\mathbf{G}_j^{(k)}, s_j^{(k)}\}_{j=1}^{M'}} \{\mathbf{c}_{i,\text{left}}, \mathbf{c}_{i,\text{right}}\} \right), \quad (11)$$

and set $\epsilon_k = 0$ if the sample is globally rejected or yields no surviving grasps.

From $\{\epsilon_k\}_{k=1}^K$ we compute

$$\bar{\epsilon} = \frac{1}{K} \sum_{k=1}^K \epsilon_k, \quad (12)$$

$$\sigma_\epsilon = \sqrt{\frac{1}{K-1} \sum_{k=1}^K (\epsilon_k - \bar{\epsilon})^2}. \quad (13)$$

We then define the LCB metric:

$$\text{LCB} = \bar{\epsilon} - z_\alpha \sigma_\epsilon. \quad (14)$$

A grasp is attempted only if $\text{LCB} > 0$, indicating that the grasp is expected to satisfy the force-closure margin with high confidence; otherwise, the system abstains. This criterion uses a one-sided lower bound, as we are specifically concerned with controlling the probability that the true grasp margin falls below zero (i.e., becomes infeasible), while any margin above zero is considered desirable. The confidence factor z_α is adjusted based on the leaf occlusion, which relaxes the bound in easier (low-occlusion) cases and becomes stricter as occlusion increases.

IV. EXPERIMENTS

A. Experimental Setup

1) *Hardware and Simulation Environments*: The system interfaces with an Intel RealSense D435i RGB-D camera mounted on a Unitree Z1 robotic arm, as shown in Fig. 3. Physical robot experiments were conducted in a controlled indoor environment arranged to replicate an indoor greenhouse strawberry plantation, with multiple hanging fruits and varied occlusion patterns.

All physical robot experiments were conducted using off-board control from the same workstation used for simulation experiments (Intel x86_64 CPU with an NVIDIA RTX 5080 GPU). Simulation experiments were performed in NVIDIA Isaac Sim, replicating the physical robot setup, including the

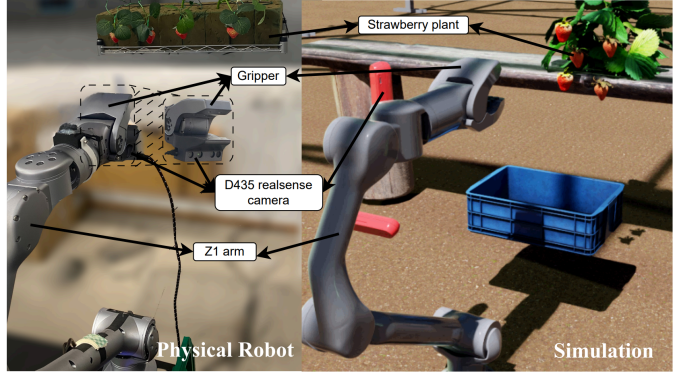


Fig. 3. (Left) Physical robot setup replicating an indoor greenhouse strawberry plantation. (Right) Simulated strawberry field in NVIDIA Isaac Sim. The strawberry plant, Unitree Z1 robotic arm, grasping mechanism, and Intel RealSense D435i RGB-D camera are annotated.

strawberry plant geometry, robot arm, gripper, and camera configuration. Identical robot hardware parameters and environmental conditions are used across simulation and physical experiments to ensure fair comparison across methods.

2) *Preprocessing and Segmentation*: Raw RGB-D point clouds are cleaned by removing invalid values (NaNs and infinities) and statistical outliers beyond three standard deviations from the median. Strawberry instances are detected using a two-stage pipeline: YOLOv8 [9] provides coarse 2D bounding boxes, which are refined using SAM2 [19] to obtain precise instance masks. Each mask is projected into 3D to extract a segmented partial point cloud \mathcal{P} corresponding to an individual strawberry.

3) *Occlusion Levels and Trial Protocol*: To systematically evaluate grasping performance under partial observability, we synthetically occlude strawberry point clouds using the geometric leaf model described in Appendix C, producing structured occlusions that resemble real leaf coverage. Experiments are conducted across five synthetically generated occlusion levels corresponding to empirical point removal rates of

$$\{0\%, 6.94 \pm 4.60\%, 28.83 \pm 12.24\%, 63.12 \pm 15.86\%, 87.45 \pm 13.86\%\}. \quad (15)$$

For each occlusion level, we perform ten trials in simulation, each consisting of grasp attempts on five strawberries, and five trials on the physical robot, each with grasp attempts on four strawberries. Across all three grasp selection strategies, this results in a total of 750 simulated grasp attempts and 300 physical robot grasp attempts.

B. Grasp Selection Strategies

As Table II illustrates, we evaluate the effectiveness of uncertainty-aware grasp selection under partial occlusion

TABLE II
EACH ROW OF THE ABLATION METHODS INDICATES WHICH COMPONENTS OF THE GRASPING PIPELINE ARE ENABLED.

Method	Shape Completion	CGNet	Geometric Filtering	Uncertainty Filtering
CGNet (Partial)	✗	✓	✗	✗
CGNet + Geometry (Partial)	✗	✓	✓	✗
Centroid (Completed)	✓	✗	✗	✗
Baseline	✓	✓	✗	✗
No Dropout	✓	✓	✓	✗
Dropout	✓	✓	✓	✓

through a controlled comparison of six grasp selection strategies: *CGNet (Partial)*, *CGNet + Geometry (Partial)*, *Centroid (Completed)*, *Baseline*, *No-Dropout*, and *Dropout*.

1) *Diagnostic Ablations*: We evaluate a small set of diagnostic ablations designed to isolate the causal contributions of individual pipeline components. These ablations are conducted in simulation only, as several variants deliberately remove safety mechanisms and would pose undue risk to the physical robot.

As summarized in the first three rows of Table II, we consider: (i) *CGNet (Partial)* where we apply CGNet directly to partial point clouds without shape completion, (ii) *CGNet + Geometry (Partial)* where we augment partial-point-cloud CGNet grasping with deterministic geometric filtering, and (iii) *Centroid (Completed)* where we implement centroid-based grasping on completed point clouds without CGNet. Together, these ablations disentangle the roles of shape completion, grasp generation, and geometric constraints under increasing occlusion.

2) *Baseline*: The baseline strategy applies CGNet to a single completed point cloud and selects the grasp with the highest predicted confidence score. No uncertainty modeling, geometric filtering, or abstention mechanism is applied, resulting in a fast but deterministic grasp selection policy.

3) *No-Dropout Selection*: The No-Dropout strategy disables dropout during point cloud completion, and therefore does not produce uncertainty estimates. As a result, only deterministic geometric grasp filters (front-facing approach, non-vertical orientation, and jaw-object intersection checks) are applied. Among the remaining grasps, the one with the highest CGNet confidence score is selected. This ablation isolates the effect of geometric filtering in the absence of uncertainty-aware reasoning.

4) *Dropout Selection (Uncertainty-Aware)*: This strategy evaluates grasp feasibility across multiple MC-dropout completion samples and applies the geometric filters used in the No-Dropout strategy in addition to uncertainty-aware filtering and the LCB decision rule described in Subsection III-C. Although repeated completion and grasp evaluation introduce additional computational cost, we apply standard engineering accelerations to ensure real-time feasibility on physical hardware; these affect runtime only and do not alter the underlying decision logic.

a) *Practical Considerations for Real-Time Deployment*: While jaw-object intersection checking contributes non-

negligible cost, the dominant runtime overhead arises from repeated point cloud completion and grasp evaluation across MC dropout samples. In real-world deployment, we optimize the jaw-object intersection test using a hierarchical strategy:

- 1) **Bounding box pre-filtering**: Axis-aligned bounding boxes are constructed around each jaw line with padding τ , allowing rapid rejection of distant points.
- 2) **Candidate restriction**: Point-to-line distance checks are performed only for points within the bounding boxes.
- 3) **Vectorized computation**: Remaining distance calculations are implemented using NumPy broadcasting, avoiding per-point Python loops.

Additional employed system-level optimizations:

- Parallel execution of MC dropout samples using thread pools.
- KD-tree acceleration for nearest-neighbor queries during contact estimation.
- Reduced the friction cone discretization, $N_{dir-opt}$, to lower the wrench computation cost.

These optimizations are not required in simulation, where execution time is less constrained, but are critical for achieving practical grasping rates on the physical robot.

C. Evaluation Metrics

We evaluate performance using grasp success rate, defined as the fraction of successful grasps over all executed attempts. An attempt corresponds to a strawberry that is successfully detected and passes all filtering stages. A grasp is considered successful if the robot securely lifts the strawberry without slippage or collision. Additional qualitative failure case analysis is provided in Appendix F. Grasp quality metrics based on contact geometry are used only internally for feasibility assessment rather than as evaluation criteria.

To isolate the effect of grasp evaluation, the grasp *position* is fixed at the centroid of the completed point cloud to ensure inverse kinematics feasibility, while uncertainty is evaluated only in the predicted grasp *orientation*. Consequently, the only difference between methods lies in how candidate grasps are evaluated and selected, allowing performance differences to be attributed directly to uncertainty-aware decision making rather than differences in perception or grasp synthesis.

D. Hyperparameters and Thresholds

Unless otherwise stated, all hyperparameters are shared across methods and fixed for all experiments.

a) *Completion and Grasp Generation*: We use an MC dropout rate of 0.1 with $K = 20$ completion samples per observation. For each completed shape, $M = 200$ candidate grasps are generated using CGNet.

b) *Geometric Constraints*: The grasp approach direction constraint $\theta_{dot} = 0.7$ enforces that grasps approach the fruit within approximately 45° of the camera-facing direction ($\cos 45^\circ \approx 0.707$), preventing risky approaches such as the rear or side that may collide with leaves. The vertical alignment constraint $\theta_{vert} = 0.5$ limits grasps to within 60° of the vertical axis $\mathbf{z} = [0, 0, 1]^T$ to reduce fruit slippage and damage.

c) *Gripper and Contact Parameters*: Based on the gripper specifications, the jaw width is set to $w = 0.04$ m, and the jaw length is constrained to $t \in [0, 0.2]$ m. A moderate friction coefficient $\mu = 0.5$ is used to reflect stable yet gentle grasps appropriate for delicate objects such as strawberries.

To account for depth sensing uncertainty, we use a conservative clearance margin of $\tau = 5$ mm. Prior work shows that RGB-D depth noise scales with distance, with standard deviations of approximately 0.7–0.8% of the measured depth [12], corresponding to 3–6 mm at the manipulation distances considered, motivating our choice of τ .

The friction cone at the contact points is discretized into $N_{dir} = 8$ directions. In the optimized dropout variant, this is reduced to $N_{dir-opt} = 6$ to improve computational efficiency without degrading performance.

d) *Occlusion-Dependent Confidence Scaling*: The parameter $\alpha \in \{0.0, 0.1, 0.2, 0.3, 0.4\}$ controls the severity of synthetic leaf occlusion applied to the strawberry point clouds and corresponds to the occlusion levels described in Subsection IV-A3. To adapt the LCB to increasing occlusion severity, we adjust the confidence factor z as a linear function of α ,

$$z_\alpha \in \{0.75, 0.88, 1.02, 1.15, 1.28\},$$

allowing stricter confidence requirements under increasing occlusion.

e) *Uncertainty Threshold Selection*: Due to differences in sensor noise, depth quantization, and unmodeled physical effects, uncertainty distributions differ between simulation and the physical robot, making a single universal threshold impractical. We therefore select thresholds empirically for each domain. After preliminary evaluation, we set the global and local uncertainty thresholds to $\delta_{global} = \delta_{local} = 0.01$ in simulation. For the physical robot experiments, we apply a stricter threshold of $\delta_{global} = \delta_{local} = 0.0037$ to account for increased sensing noise. These thresholds are fixed across all occlusion levels and trials.

V. RESULTS AND DISCUSSION

As discussed in Section II, we do not perform direct quantitative comparison with prior uncertainty-aware grasping methods, as our approach reasons over learned shape ambiguity under severe occlusion and supports object-level abstention, resulting in a fundamentally different decision scope. Instead, we evaluate our method through controlled ablations designed to isolate the effects of individual pipeline components.

A. Effect of Occlusion on Uncertainty

As occlusion increases, the centroid of the partial point cloud can shift substantially by up to 241.7% (Fig. 1), demonstrating that partial observations alone do not provide reliable geometric cues for grasping. Fig. 4 further shows that completion uncertainty, measured as the mean standard deviation of MC-dropout shape completions, increases monotonically with occlusion, reflecting growing geometric ambiguity in the reconstructed shape. Under heavy occlusion, the Dropout model exhibits large variability across samples, indicating multiple

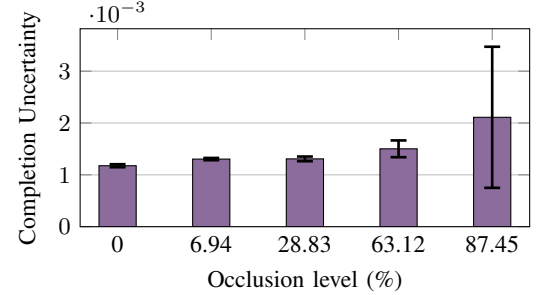


Fig. 4. Completion uncertainty under increasing occlusion. Bars indicate mean uncertainty across MC-dropout samples and whiskers denote standard deviation.

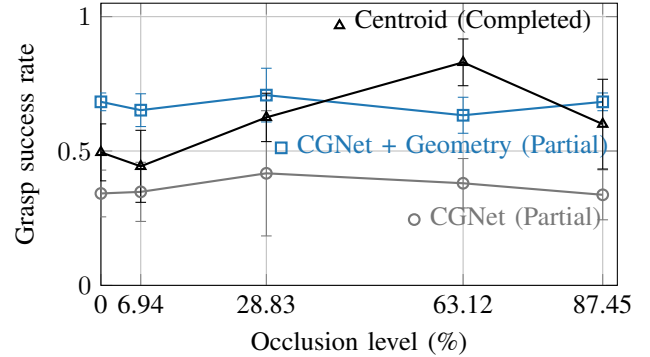


Fig. 5. Simulation-only ablations showing grasp success rate under increasing occlusion. Shape completion and geometric filtering improve robustness but remain insufficient under severe ambiguity. Values are reported as mean \pm standard deviation over ten runs.

incompatible shape hypotheses. To avoid overconfident grasp attempts under severe occlusion, we propagate completion uncertainty into grasp decision making and use an LCB-based attempt/abstain criterion.

B. Pipeline Ablations

As summarized in Fig. 5, CGNet applied directly to partial point clouds exhibits poor and inconsistent performance as occlusion increases (grey). This confirms that partial geometry alone provides insufficient information for reliable grasping in cluttered scenes.

Geometric filtering further improves robustness by eliminating physically infeasible grasps, particularly at moderate occlusion levels. Nevertheless, geometric constraints degrade under severe occlusion since they rely only on the deterministic partial point cloud, indicating that geometric heuristics alone cannot resolve ambiguity arising from missing structure.

Introducing shape completion improves performance by recovering missing geometry, even when grasps are selected using simple heuristics such as centroid-based placement. However, completion alone is insufficient under heavy occlusion, as ambiguous reconstructions can still lead to overconfident and unstable grasps if uncertainty is not explicitly quantified and incorporated into the grasp decision process.

TABLE III

GRASP SUCCESS UNDER VARYING OCCLUSION LEVELS IN SIMULATION AND PHYSICAL ROBOT EXPERIMENTS. REPORTED VALUES ARE MEAN \pm STANDARD DEVIATION.

Method	Occlusion Percentage					
	0%	6.94 \pm 4.60%	28.83 \pm 12.24%	63.12 \pm 15.86%	87.45 \pm 13.86%	Real Leaf ($\sim 70\%$)
Simulation						
CGNet (Partial)	0.342 \pm 0.087	0.348 \pm 0.110	0.417 \pm 0.233	0.380 \pm 0.092	0.337 \pm 0.093	—
CGNet + Geometry (Partial)	0.683 \pm 0.033	0.652 \pm 0.061	0.708 \pm 0.100	0.633 \pm 0.067	0.683 \pm 0.033	—
Centroid (Completed)	0.495 \pm 0.106	0.443 \pm 0.134	0.625 \pm 0.090	0.830 \pm 0.087	0.600 \pm 0.167	—
Baseline	0.580 \pm 0.227	0.585 \pm 0.263	0.647 \pm 0.197	0.690 \pm 0.247	0.760 \pm 0.107	—
No Dropout	0.675 \pm 0.216	0.777 \pm 0.174	0.710 \pm 0.196	0.730 \pm 0.228	0.780 \pm 0.129	—
Dropout	0.742 \pm 0.280	1.000 \pm 0.000	0.750 \pm 0.250	0.850 \pm 0.213	0.870 \pm 0.140	—
Physical Robot						
Baseline	0.500 \pm 0.293	0.683 \pm 0.291	0.617 \pm 0.332	0.683 \pm 0.186	0.600 \pm 0.255	0.300 \pm 0.400
No Dropout	0.500 \pm 0.274	0.733 \pm 0.389	0.600 \pm 0.374	0.467 \pm 0.400	0.483 \pm 0.170	0.367 \pm 0.371
Dropout	0.800 \pm 0.400	1.000 \pm 0.000	1.000 \pm 0.000	0.950 \pm 0.100	0.800 \pm 0.400	0.517 \pm 0.410

C. Grasp Success Under Occlusion

Compared to the three diagnostic ablations, the Baseline consistently achieves higher grasp success rates across occlusion levels, highlighting the importance of combining both shape completion and learned grasp synthesis. Methods that rely solely on partial observations (no completion model) or simple centroid-based grasping (no grasps generation model) fail under moderate to severe occlusion. This comparison demonstrates that recovering missing geometry and reasoning over learned grasp proposals are necessary prerequisites for robust grasping, even before accounting for uncertainty. The diagnostic ablations therefore motivate the Baseline as a meaningful reference point and establish that both completion and GraspNet are essential components of any effective pipeline under occlusion.

The No-Dropout method serves as an ablation that isolates the contribution of geometric filtering without uncertainty modeling. While it consistently outperforms the Baseline, a substantial gap remains relative to the full Dropout method. This gap indicates that geometric heuristics alone are insufficient under heavy occlusion. Instead, geometric filtering and uncertainty-aware selection play complementary roles: geometric constraints remove physically infeasible grasps, while uncertainty-based LCB filtering suppresses overconfident grasps arising from ambiguous perception. Robust performance under severe occlusion requires both components.

Despite increased completion uncertainty under severe occlusion (Fig. 4), the Dropout method consistently achieves higher grasp success rates than both Baseline and No-Dropout across all occlusion levels (Table III). By avoiding grasp attempts on highly ambiguous strawberries, the method prevents unsafe interactions that would otherwise lead to failed grasps or fruit damage.

VI. LIMITATIONS AND FUTURE WORKS

The proposed pipeline remains slower than fully deterministic baselines despite practical optimizations, which may limit throughput in large-scale harvesting scenarios. In addition, the system relies on single-view RGB-D observations; under extreme occlusion, insufficient visible geometry can still lead

to ambiguous completions. Grasp execution is evaluated using a fixed gripper model, which does not fully capture soft fruit compliance, friction variations, or dynamic effects.

Future work will focus on further reducing inference time, integrating active perception and next-best-view strategies to reduce uncertainty prior to grasping, and extending the approach to multi-view and multi-object harvesting. Additional strategies to further improve robustness include prioritizing the most visible or least uncertain fruits, whose removal could help clear occlusions, and actively manipulating leaves to reduce clutter.

VII. CONCLUSION

Robust robotic harvesting in agricultural environments requires reliable grasping under severe partial observability, where occlusions from leaves and neighboring fruit introduce substantial geometric uncertainty. In this work, we present an uncertainty-aware grasping pipeline for partially occluded strawberries that explicitly models uncertainty arising from learned shape completion and propagates it to grasp selection.

By combining transformer-based point cloud completion with MC dropout and a conservative LCB decision rule, the proposed method enables the robot to reason not only about grasp quality but also about confidence in that estimate. Extensive simulation and physical robot experiments show that explicitly accounting for completion uncertainty improves grasp robustness under heavy occlusion. By abstaining from grasp attempts when geometric uncertainty is high, the system reduces the risk of unstable grasps, collisions, and fruit damage.

REFERENCES

- [1] Woo-Jeong Baek, Christoph Pohl, Philipp Pelcz, Torsten Kröger, and Tamim Asfour. Improving humanoid grasp success rate based on uncertainty-aware metrics and sensitivity optimization. In *2022 IEEE-RAS 21st International Conference on Humanoid Robots (Humanoids)*, pages 786–793, 2022.
- [2] Onur Bagoren, Marc Micatka, Katherine A. Skinner, and Aaron Marburg. Pugs: Perceptual uncertainty for grasp selection in underwater environments, 2025.

[3] Angela Dai, Charles Ruizhongtai Qi, and Matthias Nießner. Shape completion using 3d-encoder-predictor cnns and shape synthesis, 2017.

[4] Nuno Ferreira Duarte, Seyed S. Mohammadi, Plinio Moreno, Alessio Del Bue, and Jose Santos-Victor. Measuring uncertainty in shape completion to improve grasp quality, 2025.

[5] C. Ferrari and J. Canny. Planning optimal grasps. In *Proceedings 1992 IEEE International Conference on Robotics and Automation*, pages 2290–2295 vol.3, 1992.

[6] Yarin Gal and Zoubin Ghahramani. Dropout as a bayesian approximation: Representing model uncertainty in deep learning, 2016.

[7] Kaijen Hsiao, Leslie Pack Kaelbling, and Tomás Lozano-Pérez. Robust grasping under object pose uncertainty. *Autonomous Robots*, 31(2):253–268, 2011.

[8] Matthias Humt, Dominik Winkelbauer, and Ulrich Hiltenbrand. Shape completion with prediction of uncertain regions, 2023.

[9] Glenn Jocher, Ayush Chaurasia, and Jing Qiu. Ultralytics yolov8, 2023.

[10] Hamidreza Kasaei and Mohammadreza Kasaei. Mv-grasp: Real-time multi-view 3d object grasping in highly cluttered environments, 2022.

[11] Ben Kehoe, Dmitry Berenson, and Ken Goldberg. Toward cloud-based grasping with uncertainty in shape: Estimating lower bounds on achieving force closure with zero-slip push grasps. In *2012 IEEE International Conference on Robotics and Automation*, pages 576–583, 2012.

[12] Kourosh Khoshelham and Sander Oude Elberink. Accuracy and resolution of kinect depth data for indoor mapping applications. *Sensors*, 12(2):1437–1454, 2012.

[13] Junggon Kim, Kunihiro Iwamoto, James Kuffner, Yasuhiro Ota, and Nancy Pollard. Physically based grasp quality evaluation under pose uncertainty. *Robotics, IEEE Transactions on*, 29:3258–3263, 04 2012.

[14] Tengyu Liu, Zeyu Liu, Ziyuan Jiao, Yixin Zhu, and Song-Chun Zhu. Synthesizing diverse and physically stable grasps with arbitrary hand structures using differentiable force closure estimator. *IEEE Robotics and Automation Letters*, 7(1):470–477, January 2022.

[15] Jens Lundell, Francesco Verdoja, and Ville Kyrki. Robust grasp planning over uncertain shape completions. In *2019 IEEE/RSJ International Conference on Intelligent Robots and Systems (IROS)*, page 1526–1532. IEEE, November 2019.

[16] Federico Magistri, Rodrigo Marcuzzi, Elias Marks, Matteo Sodano, Jens Behley, and Cyrill Stachniss. Efficient and accurate transformer-based 3d shape completion and reconstruction of fruits for agricultural robots. In *2024 IEEE International Conference on Robotics and Automation (ICRA)*, pages 8657–8663, 2024.

[17] Jeffrey Mahler, Jacky Liang, Sherdil Niyaz, Michael Laskey, Richard Doan, Xinyu Liu, Juan Aparicio Ojea, and Ken Goldberg. Dex-net 2.0: Deep learning to plan robust grasps with synthetic point clouds and analytic grasp metrics, 2017.

[18] V.-D. Nguyen. Constructing force-closure grasps. In *Proceedings. 1986 IEEE International Conference on Robotics and Automation*, volume 3, pages 1368–1373, 1986.

[19] Nikhila Ravi, Valentin Gabeur, Yuan-Ting Hu, Ronghang Hu, Chaitanya Ryali, Tengyu Ma, Haitham Khedr, Roman Rädle, Chloe Rolland, Laura Gustafson, Eric Mintun, Junting Pan, Kalyan Vasudev Alwala, Nicolas Carion, Chao-Yuan Wu, Ross Girshick, Piotr Dollár, and Christoph Feichtenhofer. Sam 2: Segment anything in images and videos, 2024.

[20] Andrea Rosasco, Stefano Berti, Fabrizio Bottarel, Michele Colledanchise, and Lorenzo Natale. Towards confidence-guided shape completion for robotic applications, 2022.

[21] Martin Sundermeyer, Arsalan Mousavian, Rudolph Triebel, and Dieter Fox. Contact-GraspNet: Efficient 6-DoF Grasp Generation in Cluttered Scenes, 2021.

[22] Andreas ten Pas, Marcus Gualtieri, Kate Saenko, and Robert Platt. Grasp pose detection in point clouds, 2017.

[23] Jun Wang, Ying Cui, Dongyan Guo, Junxia Li, Qingshan Liu, and Chunhua Shen. Pointattn: You only need attention for point cloud completion, 2022.

[24] Wentao Yuan, Tejas Khot, David Held, Christoph Mertz, and Martial Hebert. Pcn: Point completion network, 2019.

APPENDIX

A. Algorithm

The proposed UNCLE-Grasp pipeline is summarized in Algorithm 1.

B. Data Collection

We used a mixture of simulation and physical robot data to train our completion model. For simulation data, we utilized NVIDIA Isaac Sim to create a virtual strawberry field with realistic occlusions and simulated an Intel RealSense D435i RGB-D camera from the robot's perspective to capture partial point clouds of strawberries. This setup also provided complete point clouds from the simulator, which served as the ground truth for training and evaluation. Since no large-scale real-world dataset of occluded/complete strawberry pairs exists, the complete shapes were taken directly from Isaac Sim as ground truth in simulation.

For physical robot data collection, we captured RGB-D data using an Intel RealSense D435i camera in our lab environment, designed to replicate an indoor greenhouse strawberry plantation. The lab setup included five hanging strawberries with varied arrangements to simulate realistic harvesting conditions. The captured RGB-D data was processed to generate partial point clouds, which were manually annotated by aligning them with an approximated 3D CAD model. Both the simulation and physical robot environments, including the camera perspectives and strawberry field layouts, are shown in Fig. 3.

C. Synthetic Leaf Occlusion Modeling

a) Leaf Placement: A synthetic leaf is attached to one of the four lateral sides of the strawberry. The attachment axis $s \in \{x, y\}$ and sign $\sigma \in \{-1, +1\}$ are sampled uniformly at random. The leaf center \mathbf{c}_{leaf} is positioned at the corresponding boundary of the bounding box:

$$\mathbf{c}_{\text{leaf}} = \begin{cases} (x_{\max}, y_c, z_c), & \text{if } s = x, \sigma = +1 \\ (x_{\min}, y_c, z_c), & \text{if } s = x, \sigma = -1 \\ (x_c, y_{\max}, z_c), & \text{if } s = y, \sigma = +1 \\ (x_c, y_{\min}, z_c), & \text{if } s = y, \sigma = -1 \end{cases}, \quad (16)$$

where (x_c, y_c, z_c) denotes the bounding-box center.

The leaf normal \mathbf{n} points inward toward the object center, and two orthonormal vectors \mathbf{a}_1 and \mathbf{a}_2 span the leaf plane.

b) Leaf Geometry: The leaf footprint is modeled as an ellipse lying in the plane spanned by \mathbf{a}_1 and \mathbf{a}_2 . We introduce a scalar occlusion parameter α that controls the relative size of the synthetic leaf to indicate the occlusion severity. The major and minor axes of the ellipse are defined as

$$a = \alpha \cdot d, \quad b = \alpha_{\max} a. \quad (17)$$

For each point \mathbf{p}_i , we compute its coordinates in the leaf reference frame:

$$\mathbf{r}_i = \mathbf{p}_i - \mathbf{c}_{\text{leaf}}, \quad (18)$$

$$u_i = \mathbf{r}_i \cdot \mathbf{a}_1, \quad v_i = \mathbf{r}_i \cdot \mathbf{a}_2, \quad d_i = \mathbf{r}_i \cdot \mathbf{n}. \quad (19)$$

A point lies within the elliptical footprint if

$$\left(\frac{u_i}{a}\right)^2 + \left(\frac{v_i}{b}\right)^2 \leq 1. \quad (20)$$

c) Leaf Thickness: To model the finite thickness of real leaves, a point is considered occluded only if it also lies within a slab of thickness t_{leaf} along the normal direction:

$$|d_i| \leq t_{\text{leaf}}. \quad (21)$$

d) Occlusion Mask: A point \mathbf{p}_i is removed from the point cloud if it satisfies both of the following footprint and thickness constraints:

$$\mathbf{p}_i \text{ occluded} \iff \left(\frac{u_i}{a}\right)^2 + \left(\frac{v_i}{b}\right)^2 \leq 1 \wedge |d_i| \leq t_{\text{leaf}}. \quad (22)$$

The resulting occluded point cloud is given by

$$\mathcal{P}_{\text{occ}} = \{\mathbf{p}_i \in \mathcal{P} \mid \mathbf{p}_i \text{ not occluded}\}. \quad (23)$$

e) Resulting Occlusion Levels: While α controls leaf geometry, the resulting fraction of removed points depends on object shape and placement, producing a range of realistic occlusion levels from fully visible fruit to extreme coverage. Increasing occlusion can substantially shift the partial point cloud centroid (Fig. 1), motivating the use of shape completion rather than grasping directly from partial observations.

D. Training Details

The completion model was trained on 420 combined simulation and physical robot partial point cloud samples to enhance robustness and bridge the sim-to-real gap. All 67 validation and 50 test samples consist exclusively of physical robot data, ensuring evaluation under realistic sensing conditions.

Training used 1748 as a fixed seed, batch size of 16 for 400 epochs, with each point cloud uniformly sampled to 2,048 points. We employed the Adam optimizer with an initial learning rate of 1×10^{-4} , no weight decay, and applied a learning rate decay of 0.7 every 40 epochs.

At inference, the model predicts complete strawberry shapes directly from partial scans. Ground truth is not used for prediction but solely for evaluation (e.g., Chamfer Distance). The validation and test sets consist exclusively of physical robot data, ensuring that performance reflects realistic deployment scenarios. While physical robot annotations inevitably include minor manual imperfections, exposure to such noise during training improves the model's robustness in practice.

For grasp pose generation, we employ the publicly available CGNet model in an off-the-shelf manner. At inference, CGNet takes the completed point cloud predicted by our shape completion network and outputs a set of candidate grasp orientations and approach directions.

E. Vision Modules

We trained a YOLOv8 [9] model for strawberry detection using RGB images collected from both the simulation and physical robot environments. The training dataset was augmented with variations in lighting, occlusion, and strawberry orientations to improve generalization.

Although SAM2 is computationally expensive, applying it only within YOLO-predicted bounding boxes keeps the pipeline practical, which is sufficient for mobile harvesting robots where precision outweighs high frame rate. For each detected strawberry, the 2D mask is projected onto the 3D point cloud to extract the fruit-specific point cloud, \mathcal{P} , which we call the segmented partial point cloud of each strawberry. In our implementation, YOLOv8 and SAM2 require an average of 0.30 s and 0.22 s per frame, respectively, resulting in a total perception time well within the operational requirements of mobile harvesting robots.

The detected strawberries are ordered by the Euclidean distance between their estimated centers and the robot end-effector, and processed sequentially from nearest to farthest. This prioritization favors reachable targets and improves robustness under time and computational constraints.

F. Failure Case Analysis

Despite the overall improvement in grasp success achieved by the proposed uncertainty-aware pipeline, failures still occur under certain conditions. Analyzing these failure cases provides insight into the remaining limitations of the system and highlights directions for future improvement.

1) *Severe Occlusion Beyond Completion Capability.*: In cases of extreme leaf occlusion, the visible point cloud may contain insufficient geometric cues for reliable shape completion. Although the dropout-based method frequently abstains from grasping in such scenarios, occasional failures occur when multiple completion hypotheses converge to similarly incorrect shapes, leading to overconfident but inaccurate grasp estimates.

2) *Kinematic and Reachability Constraints.*: Some failures arise from the physical limitations of the robotic arm rather than perception errors. Strawberries located near the workspace boundary or partially occluded by rigid structures may admit valid grasps in perception space that are infeasible under inverse kinematics constraints, resulting in missed or unstable grasps.

3) *Execution-Level Slippage and Compliance.*: A subset of failures occurs during execution, where soft fruit compliance and unmodeled friction variations cause the strawberry to slip from the gripper despite a geometrically valid grasp. These failures are not fully captured by the geometric and force-closure metrics used in this work.

Overall, the majority of observed failures correspond to cases with high geometric uncertainty or physical execution constraints. Importantly, the proposed dropout-based strategy significantly reduces failure frequency by abstaining from grasp attempts in high-uncertainty scenarios, prioritizing safety over aggressive execution.

G. Centroid Shift Under Occlusion

To quantify the geometric bias introduced by partial occlusion, we conduct an ablation study measuring the shift in the estimated centroid of strawberry point clouds under increasing occlusion severity.

TABLE IV
AVERAGE INFERENCE TIME PER MODULE.

Method	Module	Time (s)
Shared	YOLO detection (per frame)	0.30
	SAM segmentation (per frame)	0.22
	Point cloud completion (per strawberry)	0.79
	CGNet (per strawberry)	1.57
Baseline	Grasp selection and filtering	0.01
	End-to-end (per strawberry)	2.48
No-Dropout	Filtering and selection	9.71
	End-to-end (per strawberry)	11.86
Dropout	MC completion (20 forward passes)	15.86
	CGNet (20 forward passes)	37.72
	LCB aggregation (original)	208.17
	End-to-end (original, per strawberry)	230
	LCB aggregation (optimized)	1.21
	End-to-end (optimized, per strawberry)	57.53

For each strawberry in the dataset (train/validation/test splits), we compute the centroid of the fully visible point cloud and compare it to the centroid obtained after applying synthetic leaf occlusion at each occlusion level described in Section C0e. The centroid shift is defined as the Euclidean distance between the two centroids, normalized by the bounding-box diagonal of the fully visible point cloud.

Across the entire dataset, we observe an average centroid shift of **1.86%** when comparing the fully visible case to the most severe occlusion level. As occlusion increases, centroid estimates become increasingly biased toward the visible surface regions, consistent with the qualitative example shown in Fig. 1.

This analysis highlights the fundamental limitation of centroid-based grasp localization under occlusion and motivates the use of shape completion and uncertainty-aware grasp selection. Even modest centroid shifts can result in grasp poses that are unreachable or unstable, particularly for small objects such as strawberries.

H. Inference Time

Table IV reports inference time for each module on the physical robot. While the Dropout method incurs additional computational cost due to Monte Carlo completion and grasp evaluation, optimizing the LCB aggregation stage reduces its runtime by over two orders of magnitude, resulting in an overall $4\times$ speedup compared to the unoptimized pipeline. Although uncertainty-aware grasping remains slower than deterministic baselines, this overhead represents a deliberate trade-off for increased robustness and safer behavior in highly occluded physical robot environments.

Algorithm 1 Uncertainty-aware strawberry grasping pipeline

Input:

RGB-D frame (I_{rgb}, I_d), camera model Π
 Completion network POINTATTN, grasp network CGNET
 $Mode \in \{\text{BASELINE, NODROPOUT, DROPOUT}\}$
 MC samples K , thresholds $\theta_{\text{dot}}, \theta_{\text{vert}}, \tau$
 Uncertainty thresholds $(\delta_{\text{global}}, \delta_{\text{local}})$, confidence factor z_α

Output: ATTEMPT or ABSTAIN

Perception and Segmentation

1: $\mathcal{P}_{\text{scene}} \leftarrow \text{CLEANPOINTCLOUD}(I_d)$
 2: $\{\mathcal{P}^{(j)}\}_{j=1}^J \leftarrow \text{DETECTSEGMENTPROJECT}(\text{YOLOv8, SAM2, } \Pi, \mathcal{P}_{\text{scene}})$
 3: **for** $j = 1, \dots, J$ **do**
 4: $\mathcal{P} \leftarrow \mathcal{P}^{(j)}$

Shape Completion

5: **if** mode \neq DROPOUT **then**
 6: $\mathcal{P}_{\text{completed}} \leftarrow \text{POINTATTN}(\mathcal{P})$
 7: **else**
 8: Generate $\{\mathcal{P}_{\text{completed}}^{(k)}\}_{k=1}^K$ using MC dropout
 9: **end if**

Grasp Generation

10: **if** mode \neq DROPOUT **then**
 11: $\{\mathbf{G}_i, s_i\}_{i=1}^M \leftarrow \text{CGNET}(\mathcal{P}_{\text{completed}})$
 12: **else**
 13: **for** $k = 1, \dots, K$ **do**
 14: $\{\mathbf{G}_i^{(k)}, s_i^{(k)}\}_{i=1}^M \leftarrow \text{CGNET}(\mathcal{P}_{\text{completed}}^{(k)})$
 15: **end for**
 16: **end if**

Deterministic Baselines

17: **if** mode = BASELINE **then**
 18: Execute grasp with highest s_i
 19: **return** ATTEMPT
 20: **end if**
 21: **if** mode = NODROPOUT **then**
 22: $\{\mathbf{G}_j, s_j\}_{j=1}^{M'} \leftarrow \text{GEOMFILTER}(\{\mathbf{G}_i, s_i\}_{i=1}^M, \mathcal{P}_{\text{completed}})$
 23: **if** $M' = 0$ **then**
 24: **return** ABSTAIN
 25: **else**
 26: $\mathbf{G}_{\text{selected}} \leftarrow \arg \max_{j \in \{1, \dots, M'\}} s_j$
 27: **return** ATTEMPT
 28: **end if**
 29: **end if**

Uncertainty-Aware Evaluation (Dropout)

30: **if** mode = DROPOUT **then**
 31: **if** $\text{GLOBALUNC}(\{\mathcal{P}_{\text{completed}}^{(k)}\}_{k=1}^K) > \delta_{\text{global}}$ **then**
 32: **return** ABSTAIN
 33: **end if**
 34: **for** $k = 1, \dots, K$ **do**
 35: $\{\mathbf{G}_j^{(k)}, s_j^{(k)}\}_{j=1}^{M'_k} \leftarrow \text{LOCALUNC+GEOMFILTER}(\{\mathbf{G}_i^{(k)}, s_i^{(k)}\}_{i=1}^{M_k}, \mathcal{P}_{\text{completed}}^{(k)})$ ▷
 $M'_k \leq M_k$ remaining grasps after local uncertainty and
 geometric filtering
 36: **if** $M'_k = 0$ **then**
 37: $\epsilon_k \leftarrow 0$
 38: **else**
 39: Estimate contacts for $\{\mathbf{G}_j^{(k)}\}_{j=1}^{M'_k}$
 40: $\epsilon_k \leftarrow \epsilon_{\text{FC}}(\cdot)$
 41: **end if**
 42: **end for**
 43: Compute $\bar{\epsilon}, \sigma_\epsilon$
 44: $\text{LCB} \leftarrow \bar{\epsilon} - z_\alpha \sigma_\epsilon$
 45: **if** $\text{LCB} \leq 0$ **then**
 46: **return** ABSTAIN
 47: **else**
 48: **return** ATTEMPT
 49: **end if**
 50: **end if**
 51: **end for**
 52: **return** ABSTAIN
